Computational Statistics and Data Analysis 128 (2018) 380–394

Contents lists available at ScienceDirect

Computational Statistics and Data Analysis

journal homepage: www.elsevier.com/locate/csda

Recurrence statistics for anomalous diffusion regime change detection

Grzegorz Sikora [a,*], Agnieszka Wyłomańska [a], Diego Krapf [b,c]

[a] Faculty of Pure and Applied Mathematics, Hugo Steinhaus Center, Wroclaw University of Science and Technology, Wyspianskiego 27, 50-370 Wroclaw, Poland
[b] Department of Electrical and Computer Engineering, Colorado State University, Fort Collins, CO 80523, USA
[c] School of Biomedical Engineering, Colorado State University, Fort Collins, CO 80523, USA

ARTICLE INFO

Article history:
Received 4 April 2018
Received in revised form 4 July 2018
Accepted 25 July 2018
Available online 8 August 2018

Keywords:
Segmentation
Anomalous diffusion process
Anomalous diffusion exponent
Fractional Brownian motion

ABSTRACT

For many real-time series, specific behaviors are observed where the character of the time series changes over time. This temporal evolution may indicate that some properties of the data evolve or fluctuate. One can find such problems in many different applications including physical and biological experiments as well as in technical diagnostics. From the mathematical point of view, this complexity can be considered as a segmentation problem, i.e. extraction of the homogeneous parts from the original data. Most segmentation methods assume that a simple characteristic of the time series changes, for example the mean or the variance. However, many physical applications involve a more complex situation dealing with transient statistics. Here, a new technique of the critical change point detection is introduced for the case when the data consist of anomalous diffusion processes with transient anomalous diffusion exponents. The precise mathematical formulation of a new statistics based on recurrence statistics is provided. The proposed recurrence analysis counts the number of data points falling into the appropriate circle built from consecutive observations. This approach proves to be helpful in recognizing subdiffusive and superdiffusive regions, which characterize anomalous diffusion behaviors. The main characteristics of the recurrence statistics are presented and the application to the segmentation problem is described. The effectiveness of the proposed technique is validated for a family of classical anomalous diffusive models, namely fractional Brownian motion. Finally, the methodology is applied to biological data exhibiting anomalous diffusion behavior with transient anomalous diffusion exponents.

1. Introduction

For many real data, specific behaviors that indicate the process under consideration is not homogeneous are observed. More precisely, the statistical properties of the data can change over time. In many cases, the observed time series can be modeled by a single model, albeit with a set of parameters that switches between different states. In this type of intermittent processes, an important step in the data analysis is the segmentation, i.e. the extraction of homogeneous parts with the same statistical properties. In general, the criterion for segmentation of real trajectories depends on the specific application. In some cases, the difference between states is visually recognizable, but often advanced processing is required to find the structure transition points. Thus, the key issue is to find a description of the different states that highlights their differences.

* Corresponding author.
E-mail addresses: grzegorz.sikora@pwr.wroc.pl (G. Sikora), agnieszka.wylomanska@pwr.wroc.pl (A. Wyłomańska), diego.krapf@colostate.edu (D. Krapf).

https://doi.org/10.1016/j.csda.2018.07.014
0167-9473/

In recent years, substantial works on segmentation methods for different applications appeared in the literature. A few interesting applications include condition monitoring (Crossman et al., 2003; Kucharczyk et al., 2017; Obuchowski et al., 2014), biomedical signals (e.g., electrocardiogram) (Andreao et al., 2006; Azami et al., 2012; Bhagavatula et al.; Choi and Jiang, 2008; Micó et al., 2010; Terrien et al., 2013; Vullings et al., 2000), turbulent plasmas (Gajda et al., 2013), speech analysis (Khanagha et al., 2014; Lovell and Boashash, 1988; Makowski and Hossa, 2014), econometrics (Janczura and Weron, 2013; Janczura, 2014; Tóth et al., 2010), and seismic signals (Chen, 1984; Gaby and Anderson, 1984; Kucharczyk et al., 2016; Popescu, 2014; Sokolowski et al., 2016). This problem appears also in the motion of individual molecules as observed by single-particle tracking in living cells (Gal et al., 2013; Metzler et al., 2014; Manzo and Garcia-Parajo, 2015; Krapf, 2015; Montiel et al., 2006; Krapf, 2018). Single-particle tracking measurements probe the stochastic motion of molecules as they interact with specific binding partners (Rossier et al., 2012; Weigel et al., 2013; Torreno-Pina et al., 2014; Koo and Mochrie, 2016; Yamamoto et al., 2017), move between different environments (Persson et al., 2013), are transiently confined within compartments (Fujiwara et al., 2002; Andrews et al., 2008; Albrecht et al., 2016; Sadegh et al., 2017; Krapf, 2018), or are affected by cellular activity (Caspi et al., 2000; Arcizet et al., 2008; Brangwynne et al., 2009; Katrukha et al., 2017). Additional intermittent stochastic processes arise in systems that alternate between a bulk and a surface phase (Chechkin et al., 2012; Skaug et al., 2013; Campagnola et al., 2015; Krapf et al., 2016; Wang et al., 2017) or between three-dimensional and one-dimensional types of motion (von Hippel and Berg, 1989; Loverdo et al., 2009; Bauer et al., 2015).

Many segmentation methods are based on simple statistics of the trajectories in time domain (Gajda et al., 2013; Makowski and Zimroz, 2014, 2013; Tsay, 1988; Weron et al., 2017). However, one can also find methods based on the representation of the data in different domains, such as time–frequency (Obuchowski et al., 2014; Urbanek et al., 2012). Additional methods are based on the assumption that the distribution of the displacements is known, for example, a system-level maximum-likelihood method has been employed to identify periods of confined motion within trajectories exhibiting Gaussian diffusion (Koo and Mochrie, 2016) or Gaussian anomalous diffusion (Kucharczyk et al., 2018). Universal methods to enable the identification of change points in individual trajectories have also been proposed (Lanoiselee and Grebenkov, 2017; Wagner et al., 2017; Akimoto and Yamamoto, 2017).

In this article, we focus on the segmentation problem for processes with anomalous diffusion behavior (Dumazer et al., 2017; Guantes et al., 2001; Lanoiselee and Grebenkov, 2017; Shaebani et al., 2014; Spiechowicz et al., 2016; Vazquez et al., 2001). Anomalous diffusion processes are characterized by a nonlinear mean square displacement such that $E\{X^2(t)\} = K_\beta t^\beta$ with an anomalous diffusion exponent $\beta \neq 1$ and a generalized diffusion coefficient K_β. There are two classes of the anomalous diffusion behavior: subdiffusive with $0 < \beta < 1$ and superdiffusive with $1 < \beta < 2$. However, in real-life problems we often observe anomalous diffusion behavior with transient parameters. In these cases, the time-series segmentation deals with the extraction of the parts of the trajectories with the same anomalous diffusion exponent. We introduce and give a proper mathematical formulation of a new method, based on recurrence statistics, which counts the number of data points for two-dimensional trajectories that fall into the circles built from consecutive observations. A subdiffusive random walk is more compact than a superdiffusive random walk; thus, the recurrence statistics for the two mentioned anomalous diffusion regimes are different. This observation is the base for the introduced segmentation method. We show the effectiveness of the proposed algorithm for simulated trajectories of a broad family of anomalous diffusion process, namely fractional Brownian motion, with transient anomalous diffusion exponent. The proposed methodology can also be applied to other anomalous diffusive processes with changing anomalous diffusive parameters, such as diffusion in a percolation cluster (ben Avraham and Havlin, 2000) and continuous time random walks (Lubelski et al., 2008; He et al., 2008) or other stochastic processes showing weak ergodicity breaking (Miyaguchi and Akimoto, 2011; Akimoto and Miyaguchi, 2013; Massignan et al., 2014; Albers and Radons, 2018). In this paper we prove the main properties of the introduced recurrence statistics. They can be a base for different applications of this statistics, like testing appropriate anomalous diffusive model or estimation of the anomalous diffusion parameters. This article is an extension of the authors' previous research (Sikora et al., 2017b), where the recurrence statistics was proposed as a tool to identify confined and non-confined states within experimental trajectories of molecules on the surface of live cells. This is the first time where the mathematical formulation of recurrence statistics is presented and its main statistical properties are derived and where its effectiveness is checked.

2. Anomalous diffusion processes

Many experimental data exhibit anomalous diffusion behavior. One of the tools used in anomalous diffusion recognition is the ensemble-averaged mean square displacement (EAMSD), which from the mathematical point of view is the second moment of a given process. For anomalous diffusion processes, the EAMSD fulfills a power law with respect to time, i.e.

$$\mathrm{E}\{X^2(t)\} \propto t^\beta, \tag{1}$$

where $\propto$ denotes proportionality and the parameter β is the anomalous diffusion exponent, which distinguishes between subdiffusive ($\beta < 1$), diffusive ($\beta = 1$), and superdiffusive ($\beta > 1$) regimes. Often, the available number of acquired trajectories is limited and the conventional ensemble averages over multiple realizations are replaced by time averages along a single random trajectory. As a consequence, the time-averaged mean square displacement (TAMSD) is often considered as the tool of choice for anomalous diffusion characterization.

Given a trajectory $\{X(t) : t = 1, 2, \ldots, T\}$ of length T, the TAMSD evaluated at lag time τ is defined as (Burnecki and Weron, 2010)

$$M_{X,T}(\tau) = \frac{1}{T-\tau}\sum_{t=1}^{N-\tau}[X(t+\tau) - X(t)]^2. \tag{2}$$

For ergodic processes, the TAMSD scales in the same way as the EAMSD, i.e.

$$M_{X,T}(\tau) \simeq \tau^{\beta}, \tag{3}$$

where $M_{X,T}(\tau) \simeq \tau^{\beta}$ denotes that $\mathrm{E}\{M_{X,T}(\tau)\} \propto \tau^{\beta}$ for $\tau \ll T$. For nonergodic processes, the anomalous exponent for the TAMSD (Eq. (2)) and the EAMSD (Eq. (1)) can be different. Furthermore in the nonergodic cases, while the EAMSD is a deterministic function, the TAMSD may be a random variable, even in the limit of infinite time (Metzler et al., 2014). Various methods are used for estimating β (e.g., Bayesian techniques, see Makarava et al., 2011). The most basic estimation method consists in plotting the TAMSD versus lag time in log–log scale and finding the slope by using the least squares method (Gal et al., 2013; Kepten et al., 2015). In Section 6 we apply this method to the estimation of the anomalous diffusion parameter for experimental trajectories in live cells.

Fractional Brownian motion (FBM), which can be considered as a generalization of Brownian motion, is the archetypal anomalous diffusion processes. FBM is a zero-mean Gaussian process defined as (Beran, 1994; Mandelbrot and Van Ness, 1968)

$$B_H(t) = \int_{-\infty}^{\infty}\left[(t-u)_+^{H-1/2} - (-u)_+^{H-1/2}\right]dB(u), \tag{4}$$

where $\{B(u)\}$ is the Brownian motion and $(x)_+ = \max(x, 0)$. Besides Brownian motion, FBM is the only self-similar Gaussian process with stationary increments. Furthermore, it can also be connected with fractional Langevin processes a framework for many physical systems (Lutz, 2012). Most of FBM statistical properties are characterized by the Hurst (self-similarity) exponent $0 < H < 1$. In particular, the TAMSD of FBM satisfies

$$M_{B_H,T}(\tau) \simeq \tau^{2H}, \tag{5}$$

thus $H < 1/2$ represents subdiffusive dynamics and $H > 1/2$ superdiffusive dynamics (Burnecki and Weron, 2010; Sikora et al., 2017a). The relation between Hurst exponent H and the anomalous diffusion exponent β is given by $\beta = 2H$. FBM is an ergodic process and, thus, the TAMSD for FBM converges to the EAMSD (Deng and Barkai, 2009).

This article is devoted to the segmentation method of intermittent anomalous diffusion processes. We consider intermittent FBM as a toy model in Monte Carlo simulations (see Section 5). In simple words, the intermittent FBM is the classical FBM with the alternating anomalous diffusion exponent, (Lim and Teo, 2009). The TAMSD at lag τ for a 2D process $\{(X(t), Y(t)) : t = 1, 2, \ldots, T\}$ is defined as

$$M_T(\tau) = M_{X,T}(\tau) + M_{Y,T}(\tau), \tag{6}$$

where $M_{X,T}(\tau)$ and $M_{Y,T}(\tau)$ are independent ,single-component MSD, calculated according to Eq. (2).

3. Recurrence statistics

In this section, we introduce the statistics which will be the base for the novel method of regime change for anomalous diffusion exponent. Even though the recurrence statistics can be applied in any general 2D processes, we focus on 2D Gaussian models. In our analysis, the 2D trajectory of the centered Gaussian process of length T is denoted as $\{(X(t), Y(t)) : t = 1, 2, \ldots, T\}$. It is assumed the trajectories $\{X(t) : t = 1, 2, \ldots, T\}$ and $\{Y(t) : t = 1, 2, \ldots, T\}$ are independent (2D process has two independent components). Now we define the following sequence of statistics

$$N_k := \sum_{t=1;t\neq k,k+1}^{T} \mathbf{I}\left[(X(t), Y(t)) \in C_k\right], \qquad k = 1, 2, \ldots, T-1, \tag{7}$$

where

$$\mathbf{I}\left[(X(t), Y(t)) \in C_k\right] = \begin{cases} 1, & \text{if } (X(t), Y(t)) \in C_k \\ 0, & \text{otherwise} \end{cases}$$

and C_k is the interior of the circle that connects the trajectory points $(X(k), Y(k))$ and $(X(k+1), Y(k+1))$ and is centered at the middle point of that interval, i.e. the center coordinates are $(\frac{X(k)+X(k+1)}{2}, \frac{Y(k)+Y(k+1)}{2})$

$$C_k = \left\{(x, y) \in R^2 : \left(x - \frac{X(k)+X(k+1)}{2}\right)^2 + \left(y - \frac{Y(k)+Y(k+1)}{2}\right)^2 < \frac{1}{4}\left[(X(k+1)-X(k))^2 + (Y(k+1)-Y(k))^2\right]\right\}. \tag{8}$$

The radius of that circle we denote by

$$R_k = \frac{1}{2}\sqrt{(X(k+1)-X(k))^2 + (Y(k+1)-Y(k))^2}.$$

The statistics N_k counts how many points of the 2D trajectory $\{(X(t), Y(t)) : t = 1, 2, \ldots, T\}$ fall inside the circle C_k built on trajectory points $(X(k), Y(k))$ and $(X(k+1), Y(k+1))$. Therefore $N_k \in \{0, 1, \ldots, T-2\}$. In the next subsections, we analyze the main properties of the N_k statistics for the conditions that the circle is either non-random or random.

3.1. Conditional mean of the N_k statistics

In this section, we calculate the conditional mean of the statistics N_k under the condition of non-random circle $C_k = c_k$, where c_k is built on the given trajectory points $(X(k), Y(k)) = (x(k), y(k))$ and $(X(k+1), Y(k+1)) = (x(k+1), y(k+1))$. The circle c_k is centered at $(s_k^x, s_k^y) = (\frac{x(k)+x(k+1)}{2}, \frac{y(k)+y(k+1)}{2})$ and has radius $r_k = \frac{1}{2}\sqrt{(x(k+1)-x(k))^2 + (y(k+1)-y(k))^2}$. In practical applications of our proposed method, the statistics N_k counts the trajectory points inside the generated circle. Therefore, we start by computing the conditional mean of a Gaussian process, i.e. $X(t), Y(t) \sim \mathcal{N}(0, \sigma_t^2)$.

Theorem 1. *The conditional expected value of the statistics N_k under the condition $C_k = c_k$ is given by*

$$E\{N_k | C_k = c_k\} = \sum_{t=1; t\neq k, k+1}^{T} \left(1 - Q_1\left(\sqrt{\lambda}, \frac{r_k}{\hat{\sigma}_t}\right)\right), \tag{9}$$

where

$$\begin{aligned}
\lambda &= \frac{1}{2}\left(\left(\mu_1 - s_k^x\right)^2 + \left(\mu_2 - s_k^y\right)^2\right),\\
\mu_1 &= \frac{c(t,k)c(k,k+1) - \sigma_k^2 c(t,k+1)}{c^2(k,k+1) - \sigma_k^2\sigma_{k+1}^2}x(k+1) + \frac{c(t,k)c(k,k+1) - \sigma_{k+1}^2 c(t,k)}{c^2(k,k+1) - \sigma_k^2\sigma_{k+1}^2}x(k),\\
\mu_2 &= \frac{c(t,k)c(k,k+1) - \sigma_{k+1}^2 c(t,k)}{c^2(k,k+1) - \sigma_k^2\sigma_{k+1}^2}y(k) + \frac{c(t,k)c(k,k+1) - \sigma_k^2 c(t,k+1)}{c^2(k,k+1) - \sigma_k^2\sigma_{k+1}^2}y(k+1),\\
c(i,j) &= Cov(X(i), X(j)) = Cov(Y(i), Y(j)),\\
\hat{\sigma}_t^2 &= \sigma_t^2 - c(t,k+1)\frac{c(t,k)c(k,k+1) - \sigma_k^2 c(t,k+1)}{c^2(t,k) - \sigma_k^2\sigma_{k+1}^2} - c(t,k)\frac{c(t,k)c(k,k+1) - \sigma_{k+1}^2 c(t,k)}{c^2(t,k) - \sigma_k^2\sigma_{k+1}^2},
\end{aligned}$$

and Q_M is the Marcum Q-function defined as

$$Q_M(a,b) = \int_b^\infty x\left(\frac{x}{a}\right)^{M-1}\exp\left(-\frac{x^2+a^2}{2}\right)I_{M-1}(ax)dx,$$

and I_{M-1} is the modified Bessel function of the first kind of order $M-1$

$$I_{M-1}(x) = \sum_{m=0}^{\infty}\frac{1}{m!\,\Gamma(m+M)}\left(\frac{x}{2}\right)^{2m+M-1}.$$

Proof. From the definition of N_k,

$$\begin{aligned}
E\{N_k | C_k = c_k\} &= E\left\{\sum_{t=1; t\neq k, k+1}^{T}\mathbf{I}\left[(X(t), Y(t)) \in c_k\right] | C_k = c_k\right\} = \sum_{t=1; t\neq k, k+1}^{T} E\left\{\mathbf{I}[(X(t), Y(t)] \in c_k) | C_k = c_k\right\}\\
&= \sum_{t=1; t\neq k, k+1}^{T} P\left[(X(t), Y(t)) \in c_k | C_k = c_k\right].
\end{aligned} \tag{10}$$

The conditional probability in the rightside term in (10) is

$$P\left[(X(t), Y(t)) \in c_k | C_k = c_k\right] = P\left[(X(t), Y(t)) \in c_k | (X(k), Y(k), X(k+1), Y(k+1)) = (x(k), y(k), x(k+1), y(k+1))\right].$$

We use notation $\mathbf{X} = (X(k), Y(k), X(k+1), Y(k+1))$ for the random vector and $\mathbf{x} = (x(k), y(k), x(k+1), y(k+1))$ for the specific given vector. Thus, we have to find the conditional distribution $(X(t), Y(t)) \mid \mathbf{X} = \mathbf{x}$. The vector $(X(t), Y(t), X(k), Y(k), X(k+$

1), $Y(k+1))$ is a centered Gaussian random vector with the covariance matrix

$$\Sigma_6 = \begin{bmatrix} \sigma_t^2 & 0 & c(t,k) & 0 & c(t,k+1) & 0 \\ 0 & \sigma_t^2 & 0 & c(t,k) & 0 & c(t,k+1) \\ c(t,k) & 0 & \sigma_k^2 & 0 & c(k,k+1) & 0 \\ 0 & c(t,k) & 0 & \sigma_k^2 & 0 & c(k,k+1) \\ c(t,k+1) & 0 & c(k,k+1) & 0 & \sigma_{k+1}^2 & 0 \\ 0 & c(t,k+1) & 0 & c(k,k+1) & 0 & \sigma_{k+1}^2 \end{bmatrix},$$

where $c(i,j) = Cov(X(i), X(j)) = Cov(Y(i), Y(j))$. Let us consider the following partition of the covariance matrix Σ_6 for submatrices with corresponding sizes

$$\Sigma_6 = \begin{bmatrix} \Sigma_{1,1} & \Sigma_{1,2} \\ \Sigma_{2,1} & \Sigma_{2,2} \end{bmatrix} = \begin{bmatrix} 2x2 & 2x4 \\ 4x2 & 4x4 \end{bmatrix}, \text{ so e.g. } \Sigma_{1,1} = \begin{bmatrix} \sigma_t^2 & 0 \\ 0 & \sigma_t^2 \end{bmatrix}.$$

According to the theory of multivariate Gaussian distributions, the conditional distribution

$$(X(t), Y(t)) \mid \mathbf{X} = \mathbf{x} \tag{11}$$

is a 2D Gaussian distribution with mean

$$\begin{aligned} \boldsymbol{\mu} &= \Sigma_{12}\Sigma_{22}^{-1}\mathbf{x}^T = \begin{bmatrix} c(t,k) & 0 & c(t,k+1) & 0 \\ 0 & c(t,k) & 0 & c(t,k+1) \end{bmatrix} \\ &\quad \times \begin{bmatrix} \sigma_k^2 & 0 & c(k,k+1) & 0 \\ 0 & \sigma_k^2 & 0 & c(k,k+1) \\ c(k,k+1) & 0 & \sigma_{k+1}^2 & 0 \\ 0 & c(k,k+1) & 0 & \sigma_{k+1}^2 \end{bmatrix}^{-1} \begin{bmatrix} x(k) \\ y(k) \\ x(k+1) \\ y(k+1) \end{bmatrix} \\ &= \begin{bmatrix} c(t,k) & 0 & c(t,k+1) & 0 \\ 0 & c(t,k) & 0 & c(t,k+1) \end{bmatrix} \\ &\quad \times \begin{bmatrix} \frac{\sigma_{k+1}^2}{\sigma_k^2\sigma_{k+1}^2 - c^2(k,k+1)} & 0 & \frac{c(k,k+1)}{c^2(k,k+1) - \sigma_k^2\sigma_{k+1}^2} & 0 \\ 0 & \frac{\sigma_{k+1}^2}{\sigma_k^2\sigma_{k+1}^2 - c^2(k,k+1)} & 0 & \frac{c(k,k+1)}{c^2(k,k+1) - \sigma_k^2\sigma_{k+1}^2} \\ \frac{c(k,k+1)}{c^2(k,k+1) - \sigma_k^2\sigma_{k+1}^2} & 0 & \frac{\sigma_k^2}{\sigma_k^2\sigma_{k+1}^2 - c^2(k,k+1)} & 0 \\ 0 & \frac{c(k,k+1)}{c^2(k,k+1) - \sigma_k^2\sigma_{k+1}^2} & 0 & \frac{\sigma_k^2}{\sigma_k^2\sigma_{k+1}^2 - c^2(k,k+1)} \end{bmatrix} \begin{bmatrix} x(k) \\ y(k) \\ x(k+1) \\ y(k+1) \end{bmatrix} \\ &= \begin{bmatrix} \frac{c(t,k)c(k,k+1) - \sigma_k^2 c(t,k+1)}{c^2(k,k+1) - \sigma_k^2\sigma_{k+1}^2} x(k+1) + \frac{c(t,k)c(k,k+1) - \sigma_{k+1}^2 c(t,k)}{c^2(k,k+1) - \sigma_k^2\sigma_{k+1}^2} x(k) \\ \frac{c(t,k)c(k,k+1) - \sigma_{k+1}^2 c(t,k)}{c^2(k,k+1) - \sigma_k^2\sigma_{k+1}^2} y(k) + \frac{c(t,k)c(k,k+1) - \sigma_k^2 c(t,k+1)}{c^2(k,k+1) - \sigma_k^2\sigma_{k+1}^2} y(k+1) \end{bmatrix} =: \begin{bmatrix} \mu_1 \\ \mu_2 \end{bmatrix}. \end{aligned}$$

The covariance matrix of the conditional distribution (11) has the form

$$\begin{aligned} \hat{\Sigma} &= \Sigma_{11} - \Sigma_{12}\Sigma_{22}^{-1}\Sigma_{21} = \begin{bmatrix} \sigma_t^2 & 0 \\ 0 & \sigma_t^2 \end{bmatrix} - \begin{bmatrix} c(t,k) & 0 & c(t,k+1) & 0 \\ 0 & c(t,k) & 0 & c(t,k+1) \end{bmatrix} \\ &\quad \times \begin{bmatrix} \sigma_k^2 & 0 & c(k,k+1) & 0 \\ 0 & \sigma_k^2 & 0 & c(k,k+1) \\ c(k,k+1) & 0 & \sigma_{k+1}^2 & 0 \\ 0 & c(k,k+1) & 0 & \sigma_{k+1}^2 \end{bmatrix}^{-1} \begin{bmatrix} c(t,k) & 0 \\ 0 & c(t,k) \\ c(t,k+1) & 0 \\ 0 & c(t,k+1) \end{bmatrix} \\ &= \begin{bmatrix} \sigma_t^2 & 0 \\ 0 & \sigma_t^2 \end{bmatrix} - \begin{bmatrix} c(t,k) & 0 & c(t,k+1) & 0 \\ 0 & c(t,k) & 0 & c(t,k+1) \end{bmatrix} \\ &\quad \times \begin{bmatrix} \frac{\sigma_{k+1}^2}{\sigma_k^2\sigma_{k+1}^2 - c^2(k,k+1)} & 0 & \frac{c(k,k+1)}{c^2(k,k+1) - \sigma_k^2\sigma_{k+1}^2} & 0 \\ 0 & \frac{\sigma_{k+1}^2}{\sigma_k^2\sigma_{k+1}^2 - c^2(k,k+1)} & 0 & \frac{c(k,k+1)}{c^2(k,k+1) - \sigma_k^2\sigma_{k+1}^2} \\ \frac{c(k,k+1)}{c^2(k,k+1) - \sigma_k^2\sigma_{k+1}^2} & 0 & \frac{\sigma_k^2}{\sigma_k^2\sigma_{k+1}^2 - c^2(k,k+1)} & 0 \\ 0 & \frac{c(k,k+1)}{c^2(k,k+1) - \sigma_k^2\sigma_{k+1}^2} & 0 & \frac{\sigma_k^2}{\sigma_k^2\sigma_{k+1}^2 - c^2(k,k+1)} \end{bmatrix} \begin{bmatrix} c(t,k) & 0 \\ 0 & c(t,k) \\ c(t,k+1) & 0 \\ 0 & c(t,k+1) \end{bmatrix} \\ &= \begin{bmatrix} \sigma_t^2 & 0 \\ 0 & \sigma_t^2 \end{bmatrix} \\ &\quad - \begin{bmatrix} c(t,k+1)\frac{c(t,k)c(k,k+1) - \sigma_k^2 c(t,k+1)}{c^2(t,k) - \sigma_k^2\sigma_{k+1}^2} + c(t,k)\frac{c(t,k)c(k,k+1) - \sigma_{k+1}^2 c(t,k)}{c^2(t,k) - \sigma_k^2\sigma_{k+1}^2} & 0 \\ 0 & c(t,k+1)\frac{c(t,k)c(k,k+1) - \sigma_k^2 c(t,k+1)}{c^2(t,k) - \sigma_k^2\sigma_{k+1}^2} + c(t,k)\frac{c(t,k)c(k,k+1) - \sigma_{k+1}^2 c(t,k)}{c^2(t,k) - \sigma_k^2\sigma_{k+1}^2} \end{bmatrix} \end{aligned}$$

$$= \begin{bmatrix} \sigma_t^2 - c(t,k+1)\frac{c(t,k)c(k,k+1)-\sigma_k^2 c(t,k+1)}{c^2(t,k)-\sigma_k^2\sigma_{k+1}^2} - c(t,k)\frac{c(t,k)c(k,k+1)-\sigma_{k+1}^2 c(t,k)}{c^2(t,k)-\sigma_k^2\sigma_{k+1}^2} & 0 \\ 0 & \sigma_t^2 - c(t,k+1)\frac{c(t,k)c(k,k+1)-\sigma_k^2 c(t,k+1)}{c^2(t,k)-\sigma_k^2\sigma_{k+1}^2} - c(t,k)\frac{c(t,k)c(k,k+1)-\sigma_{k+1}^2 c(t,k)}{c^2(t,k)-\sigma_k^2\sigma_{k+1}^2} \end{bmatrix}$$

$$=: \begin{bmatrix} \hat{\sigma}_t^2 & 0 \\ 0 & \hat{\sigma}_t^2 \end{bmatrix}.$$

Hence the conditional distribution (11) is 2D Gaussian $N(\boldsymbol{\mu}, \hat{\Sigma})$. Therefore probability in (10) equals to

$$\begin{aligned} P\left[(X(t), Y(t)) \in c_k | C_k = c_k\right] &= P\left[(X(t) - s_k^x)^2 + (Y(t) - s_k^y)^2 < r_k^2 | C_k = c_k\right] \\ &= P\left[\left(\frac{X(t) - s_k^x}{\hat{\sigma}_t}\right)^2 + \left(\frac{Y(t) - s_k^y}{\hat{\sigma}_t}\right)^2 < \left(\frac{r_k}{\hat{\sigma}_t}\right)^2 | C_k = c_k\right] \\ &= F_{\chi^2(2,\lambda)}\left(\left(\frac{r_k}{\sigma}\right)^2\right) = 1 - Q_1\left(\sqrt{\lambda}, \frac{r_k}{\hat{\sigma}_t}\right), \end{aligned} \tag{12}$$

where the $F_{\chi^2(2,\lambda)}$ is the cdf function of non-central $\chi^2(2, \lambda) \stackrel{d}{=} \left(\frac{X(t)-s_k^x}{\hat{\sigma}_t}\right)^2 + \left(\frac{Y(t)-s_k^y}{\hat{\sigma}_t}\right)^2$ distribution with 2 degrees of freedom and non-central parameter $\lambda = \frac{1}{2}\left(\left(\mu_1 - s_k^x\right)^2 + \left(\mu_2 - s_k^y\right)^2\right)$. That cdf is expressed by Marcum Q-function

$$Q_M(a, b) = \int_b^\infty x\left(\frac{x}{a}\right)^{M-1} \exp\left(-\frac{x^2 + a^2}{2}\right) I_{M-1}(ax)dx,$$

where I_{M-1} is modified Bessel function of the first kind of order $M - 1$

$$I_{M-1}(x) = \sum_{m=0}^{\infty} \frac{1}{m!\,\Gamma(m + M)}\left(\frac{x}{2}\right)^{2m+M-1}.$$

Summarizing we get for (10)

$$E\{N_k | C_k = c_k\} = \sum_{t=1; t\neq k, k+1}^{T} \left(1 - Q_1\left(\sqrt{\lambda}, \frac{r_k}{\hat{\sigma}_t}\right)\right). \quad \square \tag{13}$$

According to the properties of Marcum Q-function the following approximation is possible for result (13)

$$E\{N_k | C_k = c_k\} = \sum_{t=1; t\neq k, k+1}^{T} \left(1 - Q_1\left(\sqrt{\lambda}, \frac{r_k}{\hat{\sigma}_t}\right)\right) \approx \sum_{t=1; t\neq k, k+1}^{T} \Phi\left\{\frac{(\frac{(r_k/\hat{\sigma}_t)^2}{2+\lambda})^h - (1 + hp(h - 1 - 0.5(2 - h)mp))}{h\sqrt{2p}(1 + 0.5mp)}\right\}, \tag{14}$$

where Φ denotes the cdf of $\mathcal{N}(0, 1)$ and

$$h = 1 - \frac{2}{3}\frac{(2 + \lambda)(2 + 3\lambda)}{(2 + 2\lambda)^2}, \quad p = \frac{2 + 2\lambda}{(2 + \lambda)^2}, \quad m = (h - 1)(1 - 3h).$$

3.2. Mean of N_k statistics

In this part we present the formula for the average value of statistics N_k.

Theorem 2. *The expected value of the statistics N_k takes the following form*

$$E\{N_k\} = T - 2 - \sum_{t=1; t\neq k, k+1}^{T} \int_{\mathbf{R}^4} Q_1\left(\sqrt{\lambda}, \frac{r_k}{\hat{\sigma}_t}\right) f_{\mathbf{X}}(\mathbf{x})d\mathbf{x}, \tag{15}$$

where $f_{\mathbf{X}}(\mathbf{x})$ is a density of the Gaussian vector $\mathbf{X}$ with covariance matrix

$$\Sigma_4 = \begin{bmatrix} \sigma_k^2 & 0 & c(k, k+1) & 0 \\ 0 & \sigma_k^2 & 0 & c(k, k+1) \\ c(k, k+1) & 0 & \sigma_{k+1}^2 & 0 \\ 0 & c(k, k+1) & 0 & \sigma_{k+1}^2 \end{bmatrix},$$

of the form

$$f_{\mathbf{X}}(\mathbf{x}) = \frac{1}{\sqrt{(2\pi)^4 |\Sigma_4|}} \exp\left[-\frac{1}{2}\mathbf{x}\Sigma_4^{-1}\mathbf{x}^T\right], \quad \textit{where } |\Sigma_4| = \left(\sigma_k^2\sigma_{k+1}^2 - c^2(k, k+1)\right)^2,$$

and

$$-\frac{1}{2}\mathbf{x}\Sigma_4^{-1}\mathbf{x}^T = -\frac{1}{2}\left(y(k+1)\left(\frac{\sigma_k^2 y(k+1)-c(k,k+1)y(k)}{\sigma_k^2\sigma_{k+1}^2-c^2(k,k+1)}\right)+x(k+1)\left(\frac{\sigma_k^2 x(k+1)-c(k,k+1)y(k)}{\sigma_k^2\sigma_{k+1}^2-c^2(k,k+1)}\right)\right.$$
$$+\ y(k)\left(\frac{\sigma_{k+1}^2 y(k)-c(k,k+1)y(k+1)}{\sigma_k^2\sigma_{k+1}^2-c^2(k,k+1)}\right)$$
$$\left.+\ x(k)\left(\frac{\sigma_{k+1}^2 x(k)-c(k,k+1)x(k+1)}{\sigma_k^2\sigma_{k+1}^2-c^2(k,k+1)}\right)\right). \tag{16}$$

Proof. : In order to calculate the average value of statistics N_k we have to integrate the conditional mean (13) with respect to the distribution of circle C_k or equivalently vector $\mathbf{X}$. We have

$$E\,(N_k) = \int_{\mathbf{R}^4} E(N_k|C_k=c_k) f_{\mathbf{X}}(\mathbf{x})d\mathbf{x} = \sum_{t=1;t\neq k,k+1}^{T}\int_{\mathbf{R}^4} 1-Q_1\left(\sqrt{\lambda},\frac{r_k}{\hat{\sigma}_t}\right)f_{\mathbf{X}}(\mathbf{x})d\mathbf{x}$$
$$= -2-\sum_{t=1;t\neq k,k+1}^{T}\int_{\mathbf{R}^4} Q_1\left(\sqrt{\lambda},\frac{r_k}{\hat{\sigma}_t}\right)f_{\mathbf{X}}(\mathbf{x})d\mathbf{x}. \quad \square \tag{17}$$

4. Segmentation method based on recurrence statistics

The N_k statistics defined in (7) can be used as the basis of a segmentation method when the 2D trajectory corresponds to a process with changing anomalous diffusion exponent. Moreover, on the basis of the N_k statistics one can find the regime switching point, i.e. the point that divides the trajectory into two different regimes of anomalous diffusion. The idea of segmentation method is as follows. In a subdiffusion regime, a particle moves in a more compact manner than in the diffusion or superdiffusion case, i.e. the number of points that fall inside the circle C_k (see formula (8)) is larger than in case of diffusion or superdiffusion regimes. The idea is illustrated in Fig. 1 where we present two cases. The left panel corresponds to the trajectory of FBM with Hurst exponent $H = 0.05$ (subdiffusion regime). As one can observe, the number of points in the selected circle (built on consecutive observations) is much larger than in the right panel, where we present a representative trajectory of FBM with $H = 0.7$ (superdiffusive case). We also illustrate the idea of segmentation algorithm in Fig. 2. In the left panel, we present the exemplary trajectory of FBM with changing anomalous diffusion exponent. The blue parts correspond to $H = 0.05$ (subdiffusive case) and the red part to $H = 0.7$ (superdiffusive case). In the right panel, we demonstrate the N_k statistics calculated for this trajectory. The colors in the right panel correspond to the left panel. One can see the values of the N_k statistics are much smaller for the superdiffusive regime (red color) than in the subdiffusive one (blue color).

In the segmentation method for the two-dimensional observations $\{(X(t), Y(t)) : t = 1, 2, \ldots, T\}$, first we calculate the $N_k,\ k = 1, 2, \ldots, T-1$ statistics and then we find the number of points for which N_k remains below the given threshold *th*. This part of the trajectory corresponds to the diffusive or superdiffusive regime. The weak point of this method is a selection of a proper threshold. In the next section, we discuss this issue and show how the selected threshold can influence the segmentation results. In the experimental data analysis, the threshold should be selected taking into consideration the specific behavior of the analyzed data and can be different for different data sets. In order to highlight the differences of values of N_k for different anomalous diffusive regimes, we have modified the segmentation method and, instead of taking the number of points in the circle build on the consecutive observations, we propose to take under consideration three consecutive observations and calculate number of points remaining in the circle built of them. This simple modification improves the efficiency of the proposed method.

5. Monte Carlo simulations

In this section, we present the effectiveness of the segmentation method presented above, for the identification of regime-switching points for different anomalous diffusion regimes. We concentrate on fractional Brownian motion with transient anomalous diffusion exponent. This process is discussed in Section 2. Note that in the classical version, the anomalous diffusion exponent is constant.

As it was mentioned in Section 4, the selection of the threshold *th* influences the effectiveness of the segmentation. Therefore, we analyze the segmentation results for different thresholds. Moreover, the ratio between the anomalous diffusion exponent from the different regimes also influences the results. We analyze realizations of two-dimensional FBM consisting of 200 points with one transition point, i.e. two transient anomalous diffusion exponents. The first 100 points of the trajectory correspond to FBM with Hurst exponent H_1 while the next 100 points to FBM with Hurst exponent H_2. In these realizations, $H_1 < 0.5 < H_2$. Therefore, the theoretical regime switching point is 100. In Fig. 3 we present the exemplary trajectories of FBM with transient anomalous diffusion exponents for different values of H_1. The parameter H_2 is fixed and equal to 0.6.

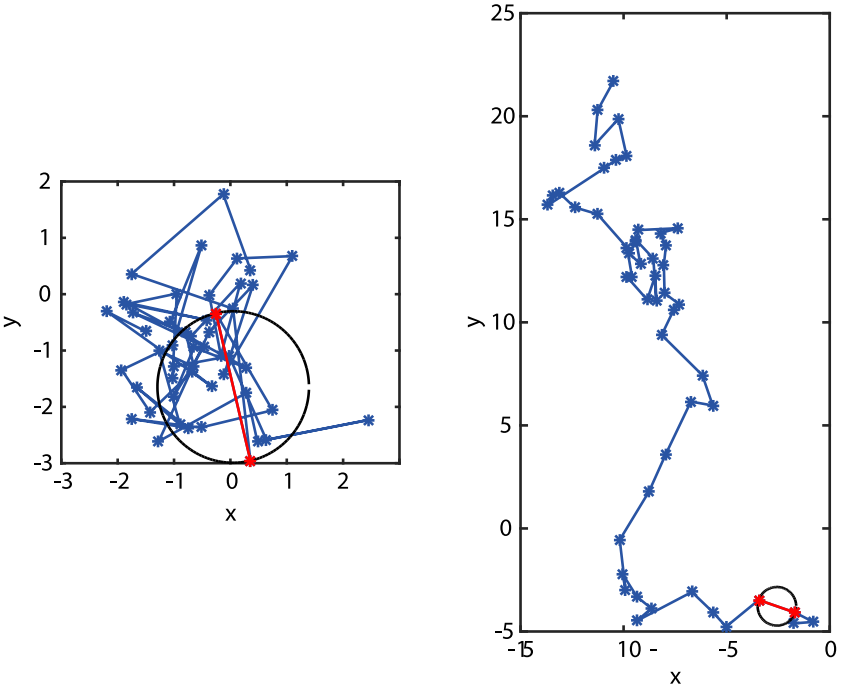

Fig. 1. Illustration of the proposed segmentation method. Left panel: FBM trajectory corresponding to the subdiffusive regime with $H = 0.05$. Right panel: FBM trajectory corresponding to the superdiffusive regime with $H = 0.7$. At each successive point pair in the time series, a circle connecting both data points and centered midway between them is drawn and the total number of data points within this circle is counted.

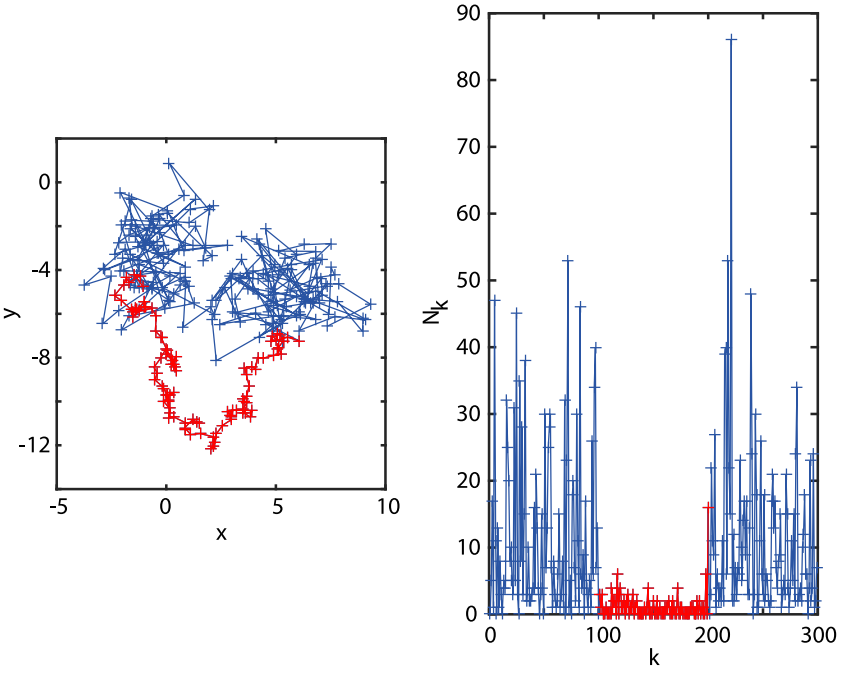

Fig. 2. Illustration of the segmentation method. Left panel: Exemplary trajectory of FBM with changing anomalous diffusion exponent. The blue parts correspond to $H = 0.05$ (subdiffusion) while the red part — to $H = 0.7$ (superdiffusion). Right panel: the N_k statistics calculated for this trajectory. The colors in the right panel correspond to the left panel. (For interpretation of the references to color in this figure legend, the reader is referred to the web version of this article.)

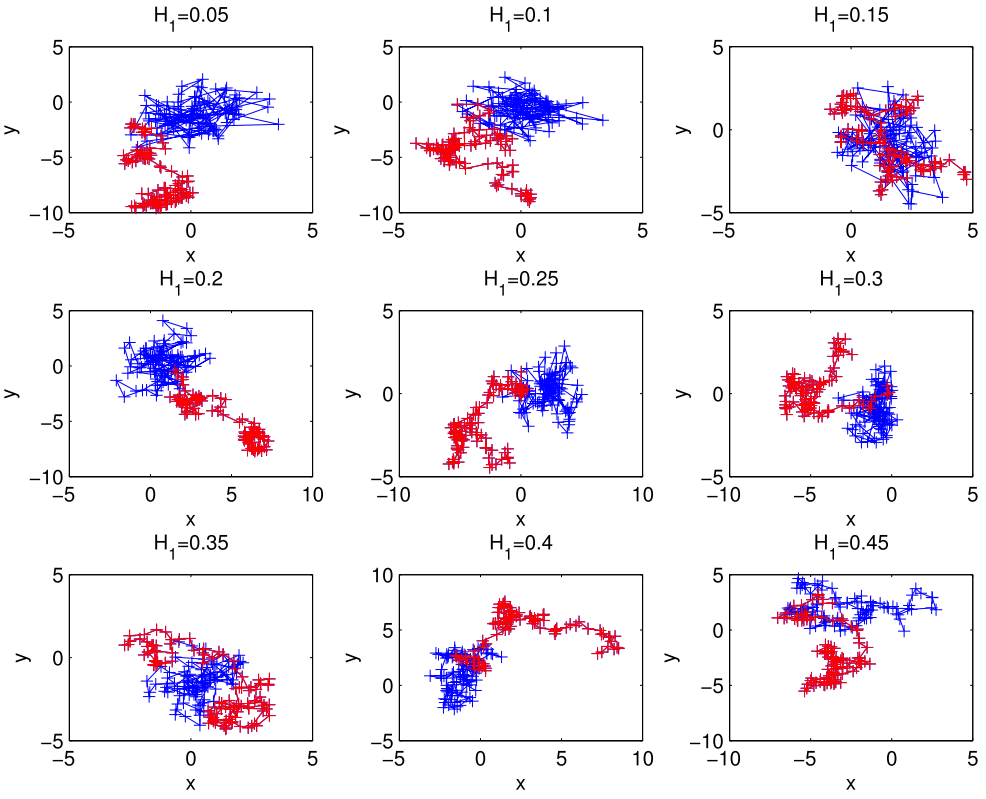

Fig. 3. Exemplary trajectories of FBM with transient anomalous diffusion exponents for different values of H_1 parameter. In all cases, we assume $H_2 = 0.6$. The part of each trajectory corresponding to the superdiffusive regime is marked in red. (For interpretation of the references to color in this figure legend, the reader is referred to the web version of this article.)

In the analysis of our Monte Carlo simulations, we use thresholds on the levels of 10%, 20%, . . . , 90%- quantiles of the N_k statistics calculated for whole 2D trajectories. We repeat the simulations 1000 times. In Fig. 4 we present the boxplots of obtained transition points for different thresholds. In each plot the nine boxplots correspond to nine considered thresholds, i.e. 10%, 20%, . . . , 90%- quantiles of N_k statistics, respectively. We consider different values of H_1, while the parameter H_2 is fixed in all cases and is equal to 0.6. As one can observe, the optimal threshold for the considered cases is the 10% quantile of all values of considered statistics. The results presented in Fig. 4 show that for larger values of the H_1 parameter, the segmentation method fails. This is the case when the ratio H_1/H_2 is close to one.

In order to show the results for other combinations of H_1 and H_2 parameters in Table 1 we compute the median of estimated regime switching point for different H_1 and H_2 parameters. The median is calculated on the basis of 1000 simulations of FBM with transient anomalous diffusion exponent. Similar as previously, the theoretical value is 100 while the number of data points in each trajectory is 200. Here we use the threshold *th* which is equal to the 10% quantile of all values of the N_k statistics for the given trajectories. Again, the method is very effective when $H_1/H_2 \ll 1$. The limitation of the method lies in the case when the ratio tends to one.

It is worth to highlight that in our simulations, we considered only the case $H_1 < 0.5 < H_2$. However, a similar study can be repeated for other cases. The presented simulation results are only illustration of the effectiveness of the proposed approach and one may use the same methodology for different anomalous diffusive models.

6. Application to experimental data

In order to illustrate the method for experimental data, we present five exemplary trajectories obtained by single-particle tracking on the surface of live cells. These trajectories correspond to fluorescently-labeled Nav1.6 sodium channels on the somatic plasma membrane of hippocampal neurons. The measurements and their statistical analysis were recently published (Akin et al., 2016; Sikora et al., 2017b). These molecules were found to transiently aggregate into nanoclusters. Interestingly, these membrane nanoclusters were hypothesized to be sites of localized channel regulation (Akin et al., 2016). Furthermore, it was found that the transient confinement of Nav1.6 channels leads to a breakdown of weak ergodicity, observed as significant differences between the time- and ensemble-averaged MSD (Weron et al., 2017). Thus, the reliable identification of transition points is an important biophysical problem. The considered 2D trajectories are illustrated in Fig. 5, left panels.

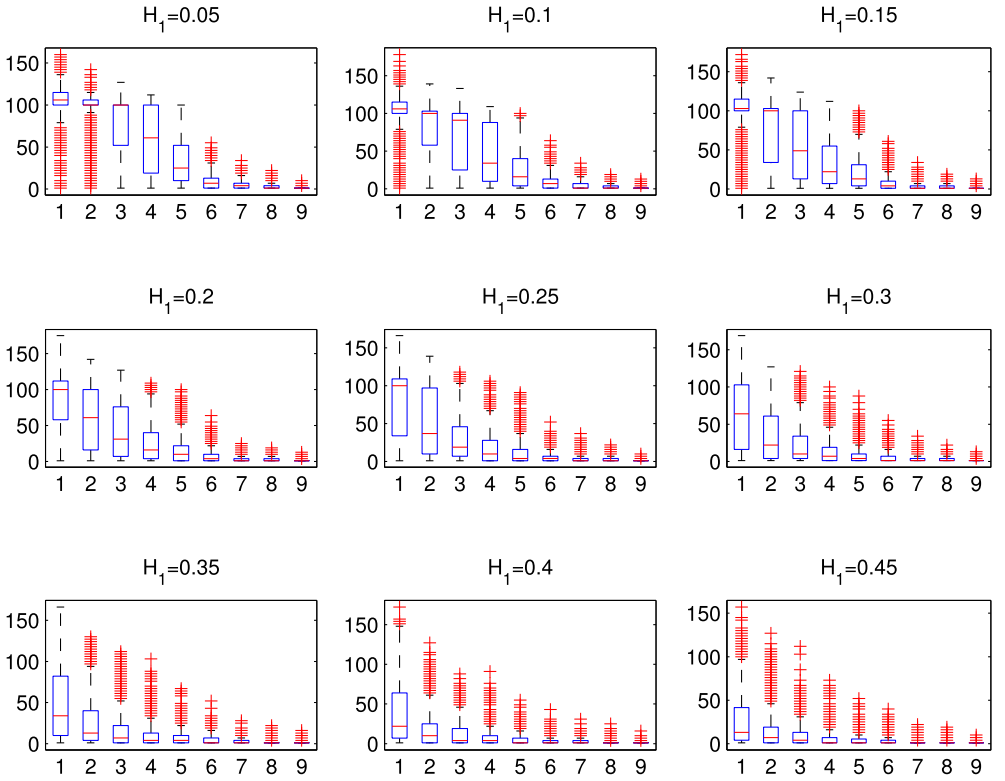

Fig. 4. The boxplots of the estimated regime switching points for FBM with transient anomalous diffusion exponent. We present the results for different values of the threshold and different values of H_1 parameter. In all cases we assume $H_2 = 0.6$. The theoretical switching point is 100. In each plot the nine boxplots correspond to nine considered thresholds, i.e. 10%, 20%, . . . , 90%- quantiles of N_k statistics, respectively.

Table 1
Median of estimated regime switching point for 1000 simulations of FBM with transient anomalous diffusion exponent. The ground truth of the switching point is 100.

H_1	H_2								
	0.55	0.6	0.65	0.7	0.75	0.8	0.85	0.9	0.95
0.05	103	103	103	103	103	103	103	100	100
0.1	100	103	103	103	103	103	100	100	100
0.15	100	100	100	103	103	103	103	100	100
0.2	97	100	100	100	103	100	100	100	100
0.25	76	97	97	100	100	100	100	100	100
0.3	40	55	85	97	97	100	100	97	97
0.35	25	35	43	79	97	97	97	97	97
0.4	13	19	31	46	52	70	73	73	82
0.45	10	10	17.5	28	37	40	40	46	43

As one can see, we may expect that the trajectories correspond to a stochastic process with transient anomalous diffusion exponent. This assumption is confirmed in Fig. 5 right panels, where we present the N_k statistics, for each considered trajectory. During some intervals of the trajectories, the N_k statistics has substantially smaller values than for the other intervals, which is indicative of changes in the anomalous diffusion exponent.

Finally, we apply the new segmentation method to the experimental 2D trajectories. In Fig. 6 (right panels) we present the segmented trajectories. The blue parts correspond to the case when the N_k statistics takes values greater than the selected threshold. Here we assume *th* equal to the 10% quantile of all values of N_k for the whole trajectory. In Fig. 6 (left panels) we demonstrate the N_k statistics with marked parts corresponding to different regimes. At the end we estimate the anomalous diffusion exponent β for 5 considered trajectories. The estimation is based on the TAMSD statistics, see (2), applied to 2D trajectories. This method is shortly described in Section 2. In Table 2 we present the estimated β parameter for segmented parts of the considered real trajectories. We take the notation $R1$-regime when N_k statistics is smaller than or equal to *th*, $R2$-regime when the N_k statistics is greater than *th*. In each case, in order to estimate the β parameter we took the longest segmented part.

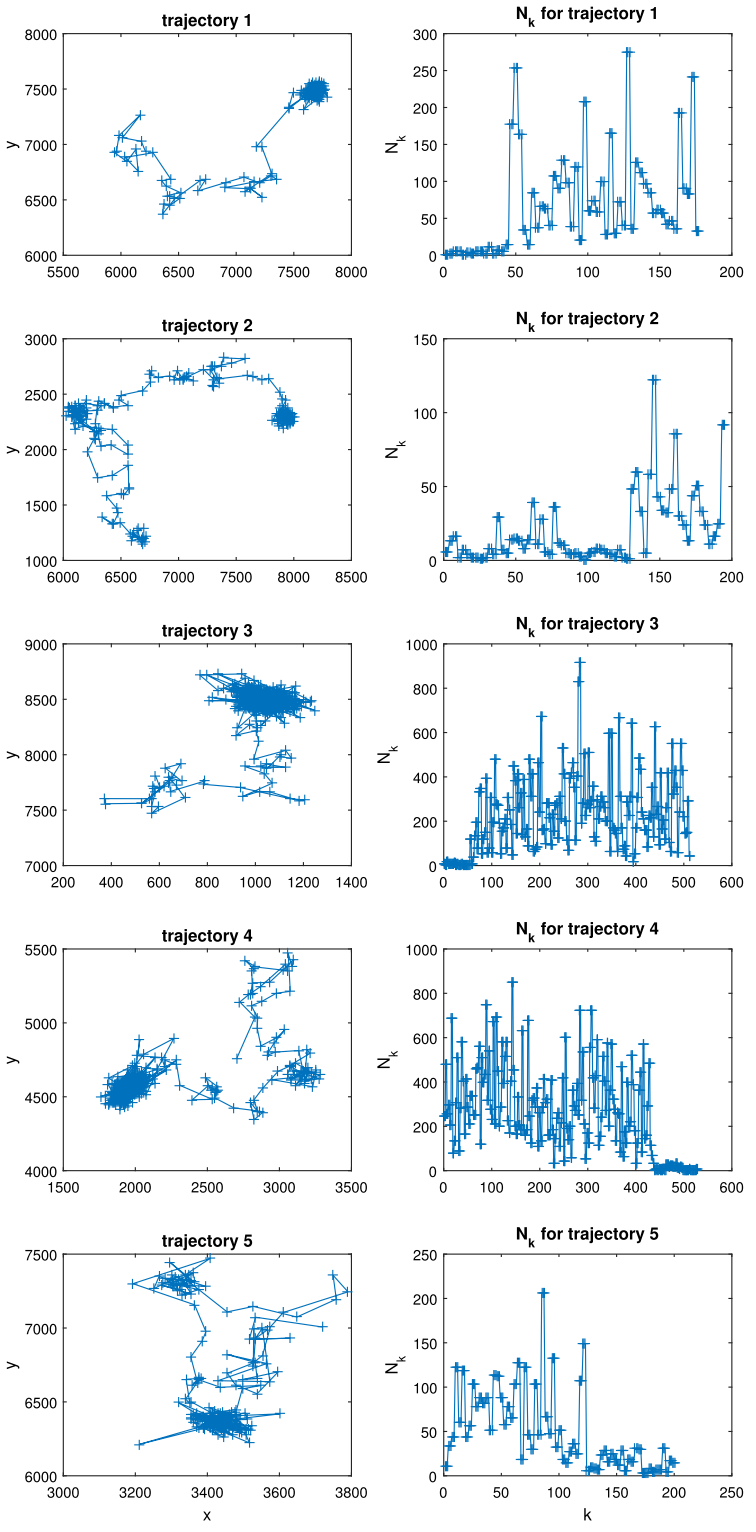

Fig. 5. The considered experimental 2D trajectories (left panels) and the corresponding N_k statistics (right panels).

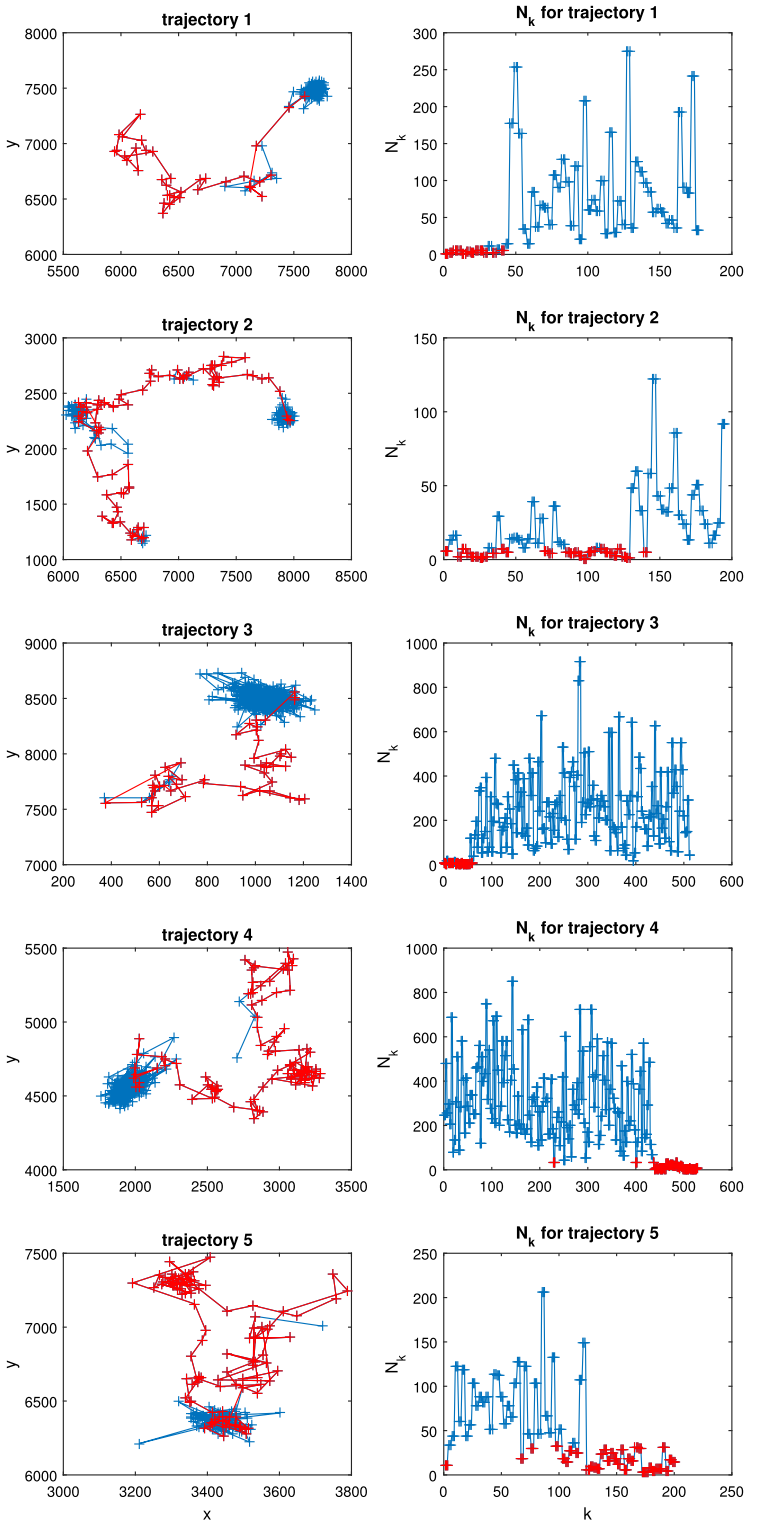

Fig. 6. Left panels: the segmented trajectories. The blue parts correspond to the case when the N_k statistics takes values greater than the threshold *th*. Right panels: the N_k statistics with marked parts corresponding to different regimes. (For interpretation of the references to color in this figure legend, the reader is referred to the web version of this article.)

Table 2
The estimated β parameter.

Trajectory	1	2	3	4	5
$\hat{\beta}$ for $R1$	1.06	1.09	0.88	0.82	0.95
$\hat{\beta}$ for $R2$	0.74	0.19	0.05	0.02	0.19

7. Conclusion

In this paper, we have introduced the recurrence statistics, which can be applied to the segmentation of 2D trajectories of anomalous diffusion processes. By segmentation, we mean extraction from the original trajectory the parts with the same anomalous diffusion exponent. The proposed statistics counts the number of data points in the trajectory that fall within the circles built from consecutive observations. The particle corresponding to subdiffusive process moves slower than in the diffusion case, while for the superdiffusive — faster. This influences the recurrence statistics and both anomalous diffusive regimes take different recurrence statistics values. The proposed segmentation technique is universal and model-free. Thus, it can be applied to any anomalous diffusion process with transient anomalous diffusion exponent without knowledge about the model. We considered the case of intermittent FBM by using numerical simulations. The same methodology can also be applied to other processes. The proposed segmentation method is also automatic as one can apply it to experimental data without deep knowledge about its details. We have presented the mathematical formulation of the recurrence statistics and calculated its main properties. We showed also how to apply it to the segmentation problem. For the classical anomalous diffusion model, namely FBM, with transient anomalous diffusion exponent, we have demonstrated the effectiveness of the novel technique and its constraints. Finally, we have applied the method to real biological data.

Acknowledgments

We thank Elizabeth Akin and Michael Tamkun for providing the measured trajectories. AW would like to acknowledge a support of National Science Center Opus Grant No. 2016/21/B/ST1/00929 "Anomalous diffusion processes and their applications in real data modelling". DK acknowledges the support of the National Science Foundation grant 1401432.

References

Akimoto, T., Miyaguchi, T., 2013. Distributional ergodicity in stored-energy-driven Lévy flights. Phys. Rev. E 87, 062134.
Akimoto, T., Yamamoto, E., 2017. Detection of transition times from single-particle-tracking trajectories. Phys. Rev. E 96 (5), 052138.
Akin, E.J., Solé, L., Johnson, B., el Beheiry, M., Masson, J.B., Krapf, D., Tamkun, M.M., 2016. Single-molecule imaging of Nav1.6 on the surface of hippocampal neurons reveals somatic nanoclusters. Biophys. J. 111 (6), 1235–1247.
Albers, T., Radons, G., 2018. Exact results for the nonergodicity of d-dimensional generalized Lévy walks. Phys. Rev. Lett. 120, 104501.
Albrecht, D., Winterflood, C.M., Sadeghi, M., Tschager, T., Noé, F., Ewers, H., 2016. Nanoscopic compartmentalization of membrane protein motion at the axon initial segment. J. Cell Biol. 215 (1), 37–46.
Andreao, R.V., Dorizzi, B., Boudy, J., 2006. ECG signal analysis through hidden Markov models. IEEE Trans. Biomed. Eng. 53 (8), 1541–1549.
Andrews, N.L., Lidke, K.A., Pfeiffer, J.R., Burns, A.R., Wilson, B.S., Oliver, J.M., Lidke, D.S., 2008. Actin restricts FcϵRI diffusion and facilitates antigen-induced receptor immobilization. Nat. Cell Biol. 10 (8), 955.
Arcizet, D., Meier, B., Sackmann, E., Rädler, J.O., Heinrich, D., 2008. Temporal analysis of active and passive transport in living cells. Phys. Rev. Lett. 101 (24), 248103.
ben-Avraham, D., Havlin, S., 2000. Diffusion and Reactions in Fractals and Disordered Systems. Cambridge University Press.
Azami, H., Mohammadi, K., Bozorgtabar, B., 2012. An improved signal segmentation using moving average and Savitzky-Golay filter. J. Signal Inf. Process. 3 (01), 39.
Bauer, M., Rasmussen, E.S., Lomholt, M.A., Metzler, R., 2015. Real sequence effects on the search dynamics of transcription factors on DNA. Sci. Rep. 5, 10072.
Beran, J., 1994. Statistics for Long-Memory Processes. Chapman & Hall.
Bhagavatula, C., Jaech, A., Savvides, M., Bhagavatula, V., Friedman, R., Blue, R., Griofa, M.O., 2012. Automatic segmentation of cardiosynchronous waveforms using cepstral analysis and continuous wavelet transforms. 19th IEEE International Conference on Image Processing, pp. 2045–2048.
Brangwynne, C.P., Koenderink, G.H., MacKintosh, F.C., Weitz, D.A., 2009. Intracellular transport by active diffusion. Trends Cell Biol 19 (9), 423–427.
Burnecki, K., Weron, A., 2010. Fractional Lévy stable motion can model subdiffusive dynamics. Phys. Rev. E 82, 021130.
Campagnola, G., Nepal, K., Schroder, B.W., Peersen, O.B., Krapf, D., 2015. Superdiffusive motion of membrane-targeting C2 domains. Sci. Rep. 5, 17721.
Caspi, A., Granek, R., Elbaum, M., 2000. Enhanced diffusion in active intracellular transport. Phys. Rev. Lett. 85 (26), 5655.
Chechkin, A.V., Zaid, I.M., Lomholt, M.A., Sokolov, I.M., Metzler, R., 2012. Bulk-mediated diffusion on a planar surface: Full solution. Phys. Rev. E 86 (4), 041101.
Chen, C., 1984. On a segmentation algorithm for seismic signal analysis. Geoexploration 23 (1), 35–40.
Choi, S., Jiang, Z., 2008. Comparison of envelope extraction algorithms for cardiac sound signal segmentation. Expert Syst. Appl. 34 (2), 1056–1069.
Crossman, J.A., Hong Guo, Y.L., Murphey, Y.L., Cardillo, J., 2003. Automotive signal fault diagnostics - Part I: Signal fault analysis, signal segmentation, feature extraction and quasi-optimal feature selection. IEEE Trans. Veh. Technol. 52 (4), 1063–1075.
Deng, W., Barkai, E., 2009. Ergodic properties of fractional Brownian-Langevin motion. Phys. Rev. E 79, 011112.
Dumazer, G., Flekkøy, E., Renard, F., Angheluta, L., 2017. Transient anomalous diffusion regimes in reversible adsorbing systems. Phys. Rev. E 96, 042106.
Fujiwara, T., Ritchie, K., Murakoshi, H., Jacobson, K., Kusumi, A., 2002. Phospholipids undergo hop diffusion in compartmentalized cell membrane. J. Cell Biol. 157 (6), 1071–1082.
Gaby, J.E., Anderson, K.R., 1984. Hierarchical segmentation of seismic waveforms using affinity. Geoexploration 23 (1), 1–16.
Gajda, J., Sikora, G., Wyłomańska, A., 2013. Regime variance testing — a quantile approach. Acta Phys. Polon. B 44 (5), 1015–1035.

Gal, N., Lechtman-Goldstein, D., Weihs, D., 2013. Particle tracking in living cells: A review of the mean square displacement method and beyond. Rheol. Acta 52 (5), 425–443.
Guantes, R., Vega, J.L., Miret-Artes, S., 2001. Chaos and anomalous diffusion of adatoms on solid surfaces. Phys. Rev. B 64, 245415.
He, Y., Burov, S., Metzler, R., Barkai, E., 2008. Random time-scale invariant diffusion and transport coefficients. Phys. Rev. Lett. 101, 058101.
Janczura, J., 2014. Pricing electricity derivatives within a Markov regime-switching model: A risk premium approach. Math. Methods Oper. Res. 79 (1), 1–30.
Janczura, J., Weron, R., 2013. Goodness-of-fit testing for the marginal distribution of regime-switching models with an application to electricity spot prices. AStA Adv. Stat. Anal. 97 (3), 239–270.
Katrukha, E.A., Mikhaylova, M., van Brakel, H.X., van Bergen en Henegouwen, P.M., Akhmanova, A., Hoogenraad, C.C., Kapitein, L.C., 2017. Probing cytoskeletal modulation of passive and active intracellular dynamics using nanobody-functionalized quantum dots. Nat. Commun. 8, 14772.
Kepten, E., Weron, A., Sikora, G., Burnecki, K., Garini, Y., 2015. Guidelines for the fitting of anomalous diffusion mean square displacement graphs from single particle tracking experiments. PLoS One 10 (2), e0117722.
Khanagha, VDaoudi K., Pont, O., Yahia, H., 2014. Phonetic segmentation of speech signal using local singularity analysis. Digit. Signal Process. 35, 86–94.
Koo, P.K., Mochrie, S.G., 2016. Systems-level approach to uncovering diffusive states and their transitions from single-particle trajectories. Phys. Rev. E 94 (5), 052412.
Krapf, D., 2015. Mechanisms underlying anomalous diffusion in the plasma membrane. In: Current Topics in Membranes, vol. 75, Academic Press, pp. 167–207.
Krapf, D., 2018. Compartmentalization of the plasma membrane. Curr Opin Cell Biol 53, 15–21.
Krapf, D., Campagnola, G., Nepal, K., Peersen, O.B., 2016. Strange kinetics of bulk-mediated diffusion on lipid bilayers. Phys. Chem. Chem. Phys. 18, 12633–12641.
Kucharczyk, D., Wyłomańska, A., Obuchowski, J., Zimroz, R., Madziarz, M., 2016. Stochastic modelling as a tool for seismic signals segmentation. Shock Vib. 2016. http://dx.doi.org/10.1155/2016/8453426.
Kucharczyk, D., Wyłomańska, A., Sikora, G., 2018. Variance change point detection for fractional Brownian motion based on the likelihood ratio test. Physica A 490, 439–450.
Kucharczyk, D., Wyłomańska, A., Zimroz, R., 2017. Structural break detection method based on the adaptive regression splines technique. Physica A 471, 499–511.
Lanoiselee, Y., Grebenkov, D.S., 2017. Unraveling intermittent features in single-particle trajectories by a local convex hull method. Phys. Rev. E 96, 022144.
Lim, S.C., Teo, L.P., 2009. Modeling single-file diffusion with step fractional Brownian motion and a generalized fractional langevin equation. J. Stat. Mech. Theory Exp. 8, 08015.
Lovell, B., Boashash, B., 1988. Segmentation of non-stationary signals with applications. In: ICASSP-88 International Conference on Acoustics, Speech, and Signal Processing, vol. 5, pp. 2685–2688.
Loverdo, C., Benichou, O., Voituriez, R., Biebricher, A., Bonnet, I., Desbiolles, P., 2009. Quantifying hopping and jumping in facilitated diffusion of DNA-binding proteins. Phys. Rev. Lett. 102 (18), 188101.
Lubelski, A., Sokolov, I.M., Klafter, J., 2008. Nonergodicity mimics inhomogeneity in single particle tracking. Phys. Rev. Lett. 100, 250602.
Lutz, E., 2012. Fractional langevin equation. In: Klafter, J., Lim, S.C., Metzler, R. (Eds.), Fractional Dynamics. Recent Advances. World Scientific, New Jersey.
Makarava, N., Benmehdi, S., Holschneider, M., 2011. Bayesian estimation of self-similarity exponent. Phys. Rev. E 84, 021109.
Makowski, R., Hossa, R., 2014. Automatic speech signal segmentation based on the innovation adaptive filter. Int. J. Appl. Math. Comput. Sci. 24 (2), 259–270.
Makowski, R., Zimroz, R., 2013. A procedure for weighted summation of the derivatives of reflection coefficients in adaptive Schur filter with application to fault detection in rolling element bearings. Mech. Syst. Signal Process. 38 (1), 65–77.
Makowski, R., Zimroz, R., 2014. New techniques of local damage detection in machinery based on stochastic modelling using adaptive Schur filter. Appl. Acoust. 77, 130–137.
Mandelbrot, B.B., Van Ness, J.W., 1968. Fractional Brownian motions, fractional noises and applications. SIAM Rev. 10, 422–437.
Manzo, C., Garcia-Parajo, M.F., 2015. A review of progress in single particle tracking: From methods to biophysical insights. Rep. Progr. Phys. 78 (12), 124601.
Massignan, P., Manzo, C., Torreno-Pina, J.A., Garcia-Parajo, M.F., Lewenstein, M., Lapeyre, G.J., 2014. Nonergodic subdiffusion from Brownian motion in an inhomogeneous medium. Phys. Rev. Lett. 112, 150603.
Metzler, R., Jeon, J.H., Cherstvy, A.G., Barkai, E., 2014. Anomalous diffusion models and their properties: Non-stationarity, non-ergodicity, and ageing at the centenary of single particle tracking. Phys. Chem. Chem. Phys. 16 (44), 24128–24164.
Micó, P., Mora, M., Cuesta-Frau, D., Aboy, M., 2010. Automatic segmentation of long-term ECG signals corrupted with broadband noise based on sample entropy. Comput. Methods Programs Biomed. 98 (2), 118–129.
Miyaguchi, T., Akimoto, T., 2011. Intrinsic randomness of transport coefficient in subdiffusion with static disorder. Phys. Rev. E 83, 031926.
Montiel, D., Cang, H., Yang, H., 2006. Quantitative characterization of changes in dynamical behavior for single-particle tracking studies. J. Phys. Chem. B 110 (40), 19763–19770.
Obuchowski, J., Wyłomańska, A., Zimroz, R., 2014. The local maxima method for enhancement of time–frequency map and its application to local damage detection in rotating machines. Mech. Syst. Signal Process. 46 (2), 389–405.
Persson, F., Lindén, M., Unoson, C., Elf, J., 2013. Extracting intracellular diffusive states and transition rates from single-molecule tracking data. Nat. Methods 10 (3), 265.
Popescu, T.D., 2014. Signal segmentation using changing regression models with application in seismic engineering. Digit. Signal Process. 24, 14–26.
Rossier, O., Octeau, V., Sibarita, J.-B., Leduc, C., Tessier, B., Nair, D., Gatterdam, V., Destaing, O., Albigés-Rizo, C., Tampé, R., Cognet, L., Choquet, D., Lounis, B., Giannone, G., 2012. Integrins $\beta 1$ and $\beta 3$ exhibit distinct dynamic nanoscale organizations inside focal adhesions. Nature Cell Biol 14, 1057–1067.
Sadegh, S., Higgins, J.L., Mannion, P.C., Tamkun, M.M., Krapf, D., 2017. Plasma membrane is compartmentalized by a self-similar cortical actin meshwork. Phys. Rev. X 7 (1), 011031.
Shaebani, M.R., Sadjadi, Z., Sokolov, I.M., Rieger, H., Santen, L., 2014. Anomalous diffusion of self-propelled particles in directed random environments. Phys. Rev. E 90, 030701(R).
Sikora, G., Burnecki, K., Wyłomańska, A., 2017a. Mean-squared displacement statistical test for fractional Brownian motion. Phys. Rev. E 95, 032110.
Sikora, G., Wyłomańska, A., Gajda, J., Solé, L., Akin, E.J., Tamkun, M.M., Krapf, D., 2017b. Elucidating distinct ion channel populations on the surface of hippocampal neurons via single-particle tracking recurrence analysis. Phys. Rev. E 96, 062404.
Skaug, M.J., Mabry, J.N., Schwartz, D.K., 2013. Single-molecule tracking of polymer surface diffusion. J. Am. Chem. Soc. 136 (4), 1327–1332.
Sokolowski, J., Obuchowski, J., Wyłomańska, A., Zimroz, R., Koziarz, E., 2016. Algorithm indicating moment of p-wave arrival based on second-moment characteristic. Shock Vib. 2016. http://dx.doi.org/10.1155/2016/4051701.
Spiechowicz, J., Łuczka, J., Hänggi, P., 2016. Transient anomalous diffusion in periodic systems: Ergodicity, symmetry breaking and velocity relaxation. Sci. Rep. 6, 30948.
Terrien, J., Germain, G., Marque, C., Karlsson, B., 2013. Bivariate piecewise stationary segmentation improved pre-treatment for synchronization measures used on non-stationary biological signals. Med. Eng. Phys. 35 (8), 1188–1196.

Torreno-Pina, J.A., Castro, B.M., Manzo, C., Buschow, S.I., Cambi, A., Garcia-Parajo, M.F., 2014. Enhanced receptor—clathrin interactions induced by N-glycan—mediated membrane micropatterning. Proc. Natl. Acad. Sci. USA 111 (30), 11037–11042.
Tóth, B., Lillo, F., Farmer, J.D., 2010. Segmentation algorithm for non-stationary compound Poisson processes. Eur. Phys. J. B 78 (2), 235–243.
Tsay, R.S., 1988. Outliers, level shifts, and variance changes in time series. J. Forecast. 7 (1), 1–20.
Urbanek, J., Barszcz, T., Zimroz, R., Antoni, J., 2012. Application of averaged instantaneous power spectrum for diagnostics of machinery operating under non-stationary operational conditions. Measurement 45 (7), 1782–1791.
Vazquez, J., Belmont, A.S., Sedat, J.W., 2001. Multiple regimes of constrained chromosome motion are regulated in the interphase Drosophila nucleus. Curr Biol 11 (16), 1227–1239.
von Hippel, P.H., Berg, O.G., 1989. Facilitated target location in biological systems. J Biol Chem 264 (2), 675–678.
Vullings, H.J.L.M., Verhaegen, M.H.G., Verbruggen, H.B., 2000. Automated ECG segmentation with dynamic time warping. In: Proceedings of the 20th Annual International Conference of the IEEE Engineering in Medicine and Biology Society, vol. 20, pp. 163–166. (1).
Wagner, T., Kroll, A., Haramagatti, C.R., Lipinski, H.-G., Wiemann, M., 2017. Classification and segmentation of nanoparticle diffusion trajectories in cellular micro environments. PLoS One 12, e0170165.
Wang, D., Wu, H., Schwartz, D.K., 2017. Three-dimensional tracking of interfacial hopping diffusion. Phys. Rev. Lett. 119 (26), 268001.
Weigel, A.V., Tamkun, M.M., Krapf, D., 2013. Quantifying the dynamic interactions between a clathrin-coated pit and cargo molecules. Proc. Natl. Acad. Sci. USA 110 (48), E4591–E4600.
Weron, A., Burnecki, K., Akin, E.J., Solé, L., Balcerek, M., Tamkun, M.M., Krapf, D., 2017. Ergodicity breaking on the neuronal surface emerges from random switching between diffusive states. Sci. Rep. 7 (1), 5404.
Yamamoto, E., Akimoto, T., Kalli, A.C., Yasuoka, K., Sansom, M.S.P., 2017. Dynamic interactions between a membrane binding protein and lipids induce fluctuating diffusivity. Sci. Adv. 3, E1601871.